Nanostructure and Viscoelasticity of Layered Silicate Nanocomposite–Electrolyte Supports

Judith Cardoso,[1] Angel Romo-Uribe,[2] Araceli Flores[3]

[1]*Área de Polímeros, Depto. de Física, DCBI Universidad Autónoma Metropolitana-Iztapalapa, Ap. Postal 55-534, México, D.F. 09340*
[2]*Laboratorio de Nanopolímeros y Coloides, Instituto de Ciencias Físicas, Universidad Nacional Autónoma de México, Ap. Postal 48-3, Cuernavaca, Mor. 62210, Mexico*
[3]*Instituto de Estructura de la Materia, C.S.I.C., Serrano 119, 28006 Madrid, Spain*

Received 20 July 2010; accepted 20 March 2011
DOI 10.1002/app.34542
Published online 9 August 2011 in Wiley Online Library (wileyonlinelibrary.com).

ABSTRACT: There is the need for novel polyelectrolytes with enhanced thermal and mechanical properties. In this report, we have reinforced a polyelectrolyte based on poly(dimethylaminoethylmethacrylate) (PDMAEM) using nanoclay montmorillonite (MMT), and have studied the thermal and viscoelastic properties. The protonated polymer (PDMAEMH) was solution mixed with functionalized MMT. Recognizing that the sort of surfactant may have a profound influence on the physical properties of the polymer matrix, neat MMT, and MMT treated with different surfactants (sulfobetaine and ammonia) were used, and the concentration of the nanofiller was varied from 1 to 5%w/w. Strikingly, while PDMAEM exhibited a glass transition temperature T_g of 32°C, the protonated PDMAEMH showed $T_g = 155$°C. Master curves obtained by applying the time-temperature superposition principle showed that PDMAEM behaved predominantly elastic ($G'' < G'$) suggesting an entangled polymer melt. However, PDMAEMH exhibited much longer relaxation times, a shift of ca. seven decades in frequency, suggesting that ionic interactions significantly hampered the molecular dynamics. X-ray scattering demonstrated that lower concentration and sulfobetaine surfactant favored exfoliation whereas ammonia and untreated MMT favored intercalation of the nanoplates. Furthermore, an enhancement in dynamic storage shear modulus was observed for the nanocomposites exhibiting intercalated morphologies relative to those displaying an exfoliated morphology. It is then suggested that the molecular dynamics is further slowed down due to confinement of the macromolecules between the nanoplates. © 2011 Wiley Periodicals, Inc. J Appl Polym Sci 123: 944–955, 2012

Key words: nanocomposites; nanostructure; polymer electrolyte

INTRODUCTION

Nanofiller-reinforced polymer composites have been the subject of wide research over the last years. These nanocomposites usually exhibit superior physical properties with respect to those of their composite counterparts. The reinforcing material can have one (nanotubes or nanofibres), two (nanosheets or nanolayers), or three dimensions (nanoparticles) in the nanometer range. Near the nanoscale filler, the polymer matrix structure and properties differ largely from those of the bulk. These effects are enhanced in nanocomposites with respect to conventional composites due to the high aspect surface-volume of the reinforcing material. The final properties of the nanofiller-reinforced composites results from a combination of the properties of the individual components and the interaction between them.

Among all the potential nanocomposite materials, those based on layered silicates have been most widely investigated for several reasons. In the first place, the starting clay materials are easily available and their intercalation chemistry has been studied for a long time.[1] In addition, this family of composite materials frequently exhibits outstanding improvements of physical properties when compared with the matrix polymers alone or equivalent micro- and macro-composite materials.[2]

Polymer-layered silicate nanocomposites are prepared by incorporating finely dispersed layered silicate materials in a polymer matrix.[3] However, dispersion of the silicate layer stacking in the polymer matrix is a difficult task further hindered by the intrinsic incompatibility of hydrophilic layered silicates and hydrophobic engineering plastics.

Correspondence to: J. Cardoso (jcam@xanum.uam.mx).
Contract grant sponsor: The MCI (Ministerio de Ciencia e Innovación), Spain; contract grant number: FIS2007-60534.
Contract grant sponsor: CONACyT (Consejo Nacional de Ciencias Y Tecnología); contract grant numbers: CB-2006-1-60686, CIAM2006/58646.
Contract grant sponsor: The UNAM-CSIC scientific exchange program.
Contract grant sponsor: DCBI, UAMI under a grant from Multidisciplinary Projects.

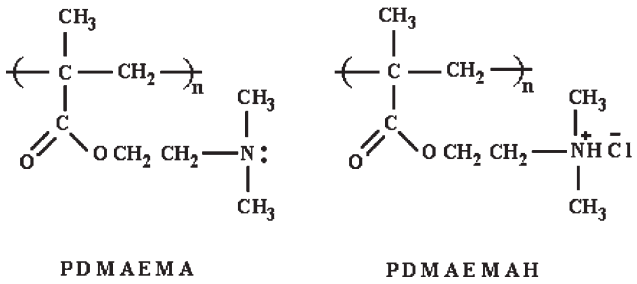

Figure 1 Chemical structure of poly (N,*N*-dimethylaminoethylmethacrylate), PDMAEMA, and protonated PDMAEMA (designated PDMAEMAH).

Therefore, layered silicates first need to be organically modified to produce polymer-compatible clays (organoclay). In fact, it has been well-demonstrated that the replacement of the inorganic exchange cations in the cavities or "galleries" of the native clay silicate structure by alkylammonium surfactants can compatibilize the surface chemistry of the clay and a hydrophobic polymer matrix.[4]

The most commonly used clay in the synthesis of polymer nanocomposites is montmorillonite (MMT), which is the major constituent of bentonite. The crystal lattice of MMT consists of a two-dimensional, $\approx$ 1 nm thick layers constituted by two tetrahedral sheets of silica (SiO_2) fused to an edge-shaped octahedral sheet of alumina where the octahedral site is isomorphically substituted.[5] The silica platelets can achieve hundreds of nanometers in length and width, with the majority within the range 200–400 nm after purification. A single gram of clay contains over a million of individual nanosized platelets.[6]

Polymer electrolytes are materials that have attracted great attention based on their vast applications in the development of solid state ionic. In a solid-state battery, solid polymer electrolytes must function both as electrolyte and as separator. Therefore, they have to meet not only requirements such as high ionic conductivity, wide electrochemical stability windows, easy processability, and lightweight, but also acceptable thermal and mechanical properties.[1,7–10] Intercalating polymer chains within layered clay hosts can produce polymer electrolyte composites with considerable interfacial area. In recent years, much work has been devoted to the melting intercalation of modified clay into the poly(ethylene oxide) (PEO) matrix.[11–13] The relationship between the thermal, electrical, and mechanical properties of composite polymer electrolytes has been investigated by Fan et al.[11] Such clay/PEO composites exhibit high conductivity and high cation transfer, and they could be processed into flexible films. By adding a small amount of MMT into PEO based electrolytes, the ionic conductivity of the electrolyte nanocomposite was enhanced relative to the neat polymer.

Recently, a new class of polymer electrolytes based on poly(dimethylaminoethylmethacrylate) (herein named PDMAEM) has been recently synthesized offering new routes for solid state ionics. The PDMAEM matrix, its protonated polymer (PDMAEMH), and the nanocomposites based on PDMAEMH/MMT (PH/clay) have been studied using dielectric spectroscopy and by high resolution transmission electron microscopy (HRTEM) demonstrating exfoliation and intercalation morphologies as a function of the type of surfactant used.[14] The results suggested that the dielectric properties were a function of morphology and prompted us to further investigate the influence of nanostructure on the thermal and viscoelastic properties of these materials.

The aim of this work is to extend preceding studies on PDMAEM nanocomposites focusing on the correlation between thermal properties, viscoelastic behavior, and nanostructure. The influence of the surfactants employed to prepare organoclay fillers on the properties and structure of the final nanocomposite is discussed as compared to untreated MMT.

EXPERIMENTAL

Sample preparation

Polymer synthesis

The synthesis and characterization of N,*N*-dimethylaminoethylmethacrylate (DMAEMA) has been previously described.[14] DMAEMA was purified by vacuum distillation (84°C/15 mmHg). Bulk polymerization was carried out at 70°C for 20 h. 2,2′-azobisisobutyronitrile (AIBN) was used as radical initiator, and a yield of 92% was achieved. The obtained polymer [herein named PDMAEMA, see Fig. 1(a)] was dissolved in benzene and precipitated in cold hexane, dried in a vacuum oven at 50°C for 24 h and stored in a desiccator. PDMAEMA is an amorphous powder.

Protonated polymer preparation

PDMAEMA was dissolved in a 1*M* hydrochloric acid (HCl) solution in 1 : 1*M* ratio at room temperature and under agitation. The solution was kept in agitation overnight. The protonated polymer (herein named PDMAEMAH) was then precipitated by ethanol and washed with distilled water to get the purified salt [see Fig. 1(b)]. PDMAEMAH was also an amorphous powder.

Structure and molecular weight of pristine polymer

PDMAEMA structure was verified by 1HNMR in 5–10% weight solution of $CDCl_3$ with tetramethylsilane

(TMS) as an internal reference. δ units (ppm) were recorded. The protonated polymer was characterized by ^{1}HNMR (D_2O) and FTIR (film) spectra. Elemental analysis was used to verify the chemical composition of the polymers. Light-scattering experiments were performed at room temperature on a Dawn-F (Wyatt Tech.) apparatus at $\lambda = 6320$ Å in methanol. The refractive index increment (*dn/dc*) was calculated as 0.157 mL/g in the same solvent at the same wavelength.

Organomontmorillonite (organo-MMT) preparation

MMT used in this work has an ionic interchanged degree of 135 meq/100 g (Aldrich). Na-montmorillonite is hydrophilic and not compatible with most organic molecules. The sodium cation in the interlayer space of MMT can be exchanged with organic cations to yield organophilic MMT (organo-MMT). For the present purpose, a sulfobetaine zwitterion, dodecyldimethyl(3-sulfo-propyl) ammonium hydroxide inner salt, (C_{12}SB) was chosen as surfactant to increase the interlayer distance and facilitate the intercalation of PDMAEMAH. In a 1 L beaker were placed 24 mmol of surfactant, 2.4 mL of concentrated hydrochloric acid, and 200 mL of water, at 80°C. The surfactant solution was added to a dispersion composed of 10 g of MMT and 1000 mL of hot water, and then this mixture was stirred vigorously for 2 h, yielding a pink precipitate. The product was filtered, repeatedly washed with distilled water to remove the excess intercalative reagent, dried in a vacuum oven at 50°C for 48 h and stored in a desiccator. Under these conditions, C_{12}SB shows a cationic behavior.

Nanocomposites preparation

Dispersions of 0.17 g of MMT or organo-MMT were prepared in 10 mL of distilled water, and then a solution composed of 3.17 g PDMAEMAH and 10 mL of distilled water was slowly added. The mixture was stirred for 48 h at room temperature. The obtained nanocomposite was dried in a vacuum oven at 40°C to obtain a constant weight. The nanocomposite with nanoclay (PH/MMT/C_{12}SB) was kept in a desiccator. The same preparation procedure was used for the other nanocomposites compositions when using either surfactant.

Thermal properties

The thermal transitions were determined using a MDSC2920 modulated differential scanning calorimeter manufactured by TA Instruments (Newcastle, DE). Modulated DSC scans were carried out at 5°C/min with amplitude of ± 0.5°C and a period of 40 s. Two scans of similar samples were employed to determine the glass transition temperature T_g for each material. Decomposition temperatures were determined using a Thermal Analysis Thermogravimetry instrument TGA2950 linked to a Thermal Analyzer 2100 microprocessor (TA Instruments, Newcastle, DE). The TGA scans were carried out at a heating rate of 10°C/min under 50 mL/min nitrogen flow.

Rheology

Small-strain oscillatory shear measurements were carried out using the stress-controlled CVO rheometer manufactured by Malvern Instruments (United Kingdom). Parallel plate's fixtures of 25 mm diameter were used. Strain sweeps were carried out to determine the linear viscoelastic (LVE) regime of each sample. However, frequency sweeps, within the LVE regime, were carried out over a range of temperatures to apply the time-temperature superposition principle. Thermal transitions were determined carrying out dynamic temperature scans in shearing mode at 1 rad/s, applying a heating rate of 2°C/min.

X-ray scattering

Two-dimensional patterns were obtained using a Micro Star rotating anode generator with copper target manufactured by Bruker (Germany). Middle-angle X-ray scattering (MAXS) patterns were recorded using a Mar345 dtb image plate with a resolution of 3450 × 3450 pixels, and 100 μm/pixel; a sample-to-detector distance of 40 cm was used. The patterns were analyzed using the X-ray scattering software POLAR® v2.6 (Stonybrook Technology and Applied Research, NY).

RESULTS AND DISCUSSION

The structure of PDMAEMA and PDMAEMAH (Fig. 1) was characterized by ^{1}H-NMR; the results are summarized in Table I. At around 3 ppm appeared the proton of the ammonium group together with $(CH_3)_2N + H$—. The fast Fourier transform infrared, FTIR, spectrum obtained from a film cast from chloroform ($CHCl_3$) showed the ν_{max} in 2960 and 2926 (C—H saturated), 1720 (C=O), 1456 (CH3—), 1400, 1290, 1176 (C—O ester group), and 1100 (C—O ether group) cm^{-1}. However, elemental analysis showed the following results: C 59.97%, H 9.60%, and N 8.83% calculated for $C_8H_{15}NO_2.2H_2O$, C 59.70%, H 9.50%, and N 8.69%. The weight average molecular weight, $\bar{M}_w$ determined in ethanol (CH_3OH) by light scattering, was 6.28×10^4 Da.

However, the FTIR spectrum of PDMAEMAH showed the same ν_{max} as PDMAEMA plus a strong

TABLE I
Assignation of ^{1}H NMR Signals of PDMAEMA and PMAEMAH

PDMAEMA δ (ppm)	PDMAEMAH δ (ppm)
0.907 and 1.159	0.997–1.136
(3H, 2s, —CH_3)	(3H, 2s, —CH_3),
1.822–1.947	2.02
(2H, 3s, —$\underline{CH_2}$—C(CH_3)	(2H, 3s, —$\underline{CH_2}$—C(CH_3)
2.284	2.942–3.022
(6H, s, $(CH_3)_2$—N)	(6.7H, m, $(\underline{CH_3})_2$—N^+) + H2O
2.566	3.57
(2H, s, —CH_2—N)	(2H, s, —CH_2—N^+)
4.055	4.246
(2H, t, CH_2—O)	(2H, t, CH_2—O)

resonance at 3406 y1640 cm^{-1}, which was assigned to H_2O adsorbed and 2690 cm^{-1} assigned to the —$N^+H(CH_3)_2$ group. The elemental analysis of PDMAEMAH showed: C 48.10%, H 9.38%, and N 6.54%, calculated for the repetitive unit $C_8H_{16}NO_2$.2.1 H_2O C 49.28%, H 9.29%, and N 7.18%.

Thermal properties

Relatively thick films, about 2 mm thick, of the polymer and its nanocomposites were cast from aqueous solutions. Figure 2 shows photographs of the films under white light conditions. There can be seen that the relatively thick films are optically transparent, and there is no evidence for nanoclay agglomeration suggesting good nanoclay dispersion within the polymer matrix. It should be pointed out that the optical micrographs do not demonstrate exfoliation or intercalation in the nanocomposites. The micrographs only suggest good dispersion of the nanoclays in the polymer matrix because the nanocomposites maintained optical transparency, as the neat polymer. However, one of us has already reported HRTEM demonstrating conclusively exfoliation and intercalation in the nanocomposites, and the type of nanostructure is dependent on the surfactant used to treat the nanoclay, as will be further discussed below.[14]

Thermogravimetric analysis data revealed that the samples were hygroscopic; however there was a clear influence of the nanoclay on the material's hygroscopic properties. The humidity values for all samples are reported in Table II. The amount of humidity for the neat polymer was 16% g/g. However, the level of humidity was reduced with the addition of nanoclay. Note that the nanocomposite containing 3 wt % of MMT treated with sulfobetaine exhibited

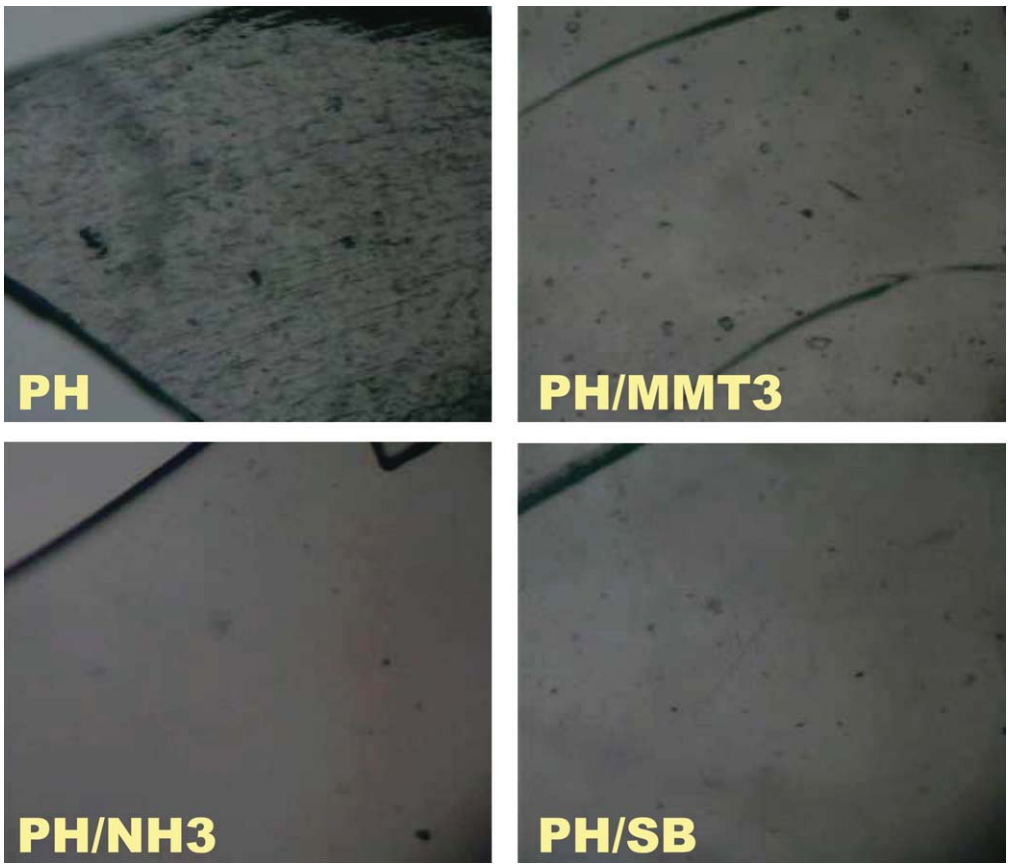

Figure 2 Photographs of films prepared from PDMAEMA, PDMAEMAH, and their layered silicate nanocomposites. [Color figure can be viewed in the online issue, which is available at wileyonlinelibrary.com.]

TABLE II
Pristine, Protonated Polymers, and the Layered Silicate Nanocomposites

Sample	Material	MMT (wt %)	H_2O (wt %)
P	PDMAEMA	0	16
PH	PDMAEMAH	0	15
PH/3MMT	PDMAEMAH/MMT	3	13
PH/MMT/1NH	PH/MMT/$C_{14}NH_4^+$	1	14
PH/MMT/3NH	PH/MMT/$C_{14}NH_4^+$	3	13
PH/MMT/5NH	PH/MMT/$C_{14}NH_4^+$	5	15
PH/MMT/1SB	PH/MMT/$C_{12}SB$	1	14
PH/MMT/3SB	PH/MMT/$C_{12}SB$	3	10
PH/MMT/5SB	PH/MMT/$C_{12}SB$	5	12

PDMAEMA, poly (N,Ndimethylaminoethylmethacrylate); PDMAEMAH (protonated PDMAEMA), MMT, montmorillonite; NH, ammonia; SB, sulphobetaine.

TABLE III
Thermal Properties of Pristine, Protonated Polymers, and the Nanocomposites

Sample	$T_{g,DSC}$ (°C)	$T_{g,DMA}$ (°C)	$T_{d,onset}$ (°C)
P	32	35	173
PH	155	164	224
PH/3MMT	162	164	210
PH/MMT/1NH	163	–	231
PH/MMT/3NH	168	171	234
PH/MMT/5NH	160	–	228
PH/MMT/1SB	162	–	281
PH/MMT/3SB	158	152	285
PH/MMT/5SB	154	162	267

Glass transition temperatures determined by means of MDSC, *Tg*,DSC, and from the temperature at maximum of loss modulus *G′*, *Tg*,DMA. Degradation temperature, *Td*,onset, as determined by TGA.

the lowest level of humidity of 10 wt %. A possible explanation of the anomalous moisture uptake in our samples is associated to the immobilization of water molecules on the surfaces of the hydrophilic MMT clay layers. Pavlidou and Papaspyrides[1] have already pointed out that after a nanocomposite is immersed in water, three processes may occur: (1) sorption of water molecules on the sample surfaces, (2) diffusion of water into the sample, and (3) adsorption of water molecules on the hydrophilic surfaces of nanoclay layers, where these molecules become immobilized. Thus, when the concentration of nanoclay was increased the water absorption decreased due to the immobilization of water molecules on the surfaces of the hydrophilic MMT clay layers. Similar results were reported for polyamide 6,6 by Liu and Wu.[15] In the case of the surfactant $C_{12}SB$, its high polarity would give rise to a higher immobilization of water molecules. This would be the reason why the amount of humidity is less at the temperature recorded from TGA curves.

The decomposition temperatures, T_d, determined at 10% weight loss are listed in Table III and the influence of nanoclay concentration on T_d is shown in Figure 3. Thermally stable polymers are sought for applications in battery devices. Results show that the sulfobetaine surfactant significantly enhanced the thermal stability of the nanocomposites, in contrast to ammonia. Indeed, the decomposition temperature when using $C_{12}SB$ as surfactant increased over 100 and 56°C relative to the neat and protonated polymers, respectively. Finally, note that neat MMT also showed an increase in thermal stability when compared to the neat polymer (P), that is the decomposition temperature increased to $T_d = 210$°C. In contrast, the decomposition temperature decreased for PH/3MMT when compared with the protonated polymer PH.

It is generally observed that the incorporation of clay into a polymer matrix enhanced the thermal stability by acting as an insulator and mass transport barrier to the volatile products generated during decomposition, as well as by assisting in the formation of char after thermal decomposition.[2] When MMT is treated with an organic ammonium salt, the original inorganic MMT becomes lipophilic and the interlayer galleries obstruct the volatile gas produced by thermal decomposition. Moreover, from the viewpoint of the thermal decomposition process, thermal decomposition begins from the surface of the nanocomposites. When the molecules at the

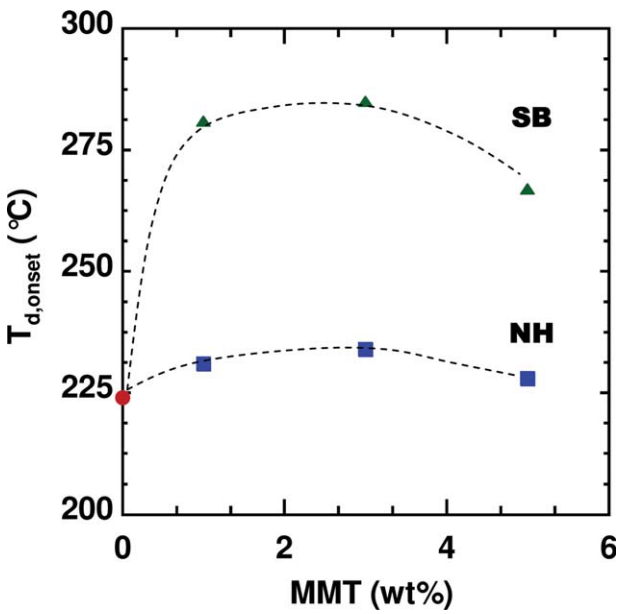

Figure 3 Onset of degradation temperature, $T_{d,onset}$, as determined by TGA as a function of concentration of montmorillonite (MMT). Data also show the influence of the sort of surfactant (ammonia, NH, or sulfobetaine, SB) used. [Color figure can be viewed in the online issue, which is available at wileyonlinelibrary.com.]

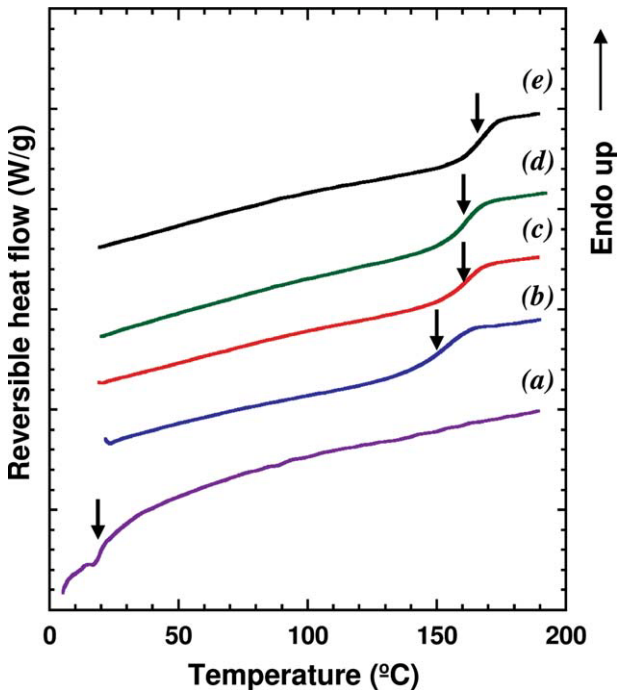

Figure 4 Modulated DSC heating scans of neat and protonated polymers and their layered silicate nanocomposites. (a) PDMAEMA, (b) PDMAEMAH, (c) PH/MMT 3 wt %, (d) PH/MMT/C_{12}SB 3 wt %, and (e) PH/MMT/$C_{14}NH_4^+$ 3 wt %. Reversible heat flow obtained from second heating scan. [Color figure can be viewed in the online issue, which is available at wileyonlinelibrary.com.]

surface of the nanocomposites decompose, the organo-MMT content increases and the clay forms a "protection layer." Therefore, PH/organo-MMT nanocomposites can exhibit better thermal stability than the protonated polymer, PH.

Due to the fact that untreated MMT favored intercalation of the nanoplates (see next section on X-ray scattering results), it could be argued that after the early stages of thermal decomposition the stacked silicate layers could hold accumulated heat, acting as a heat source to accelerate the decomposition process, in conjunction with the heat flow supplied by the external heat source, as suggested by Zhao et al.[16] Moreover, the clay itself can also catalyze the degradation of polymer matrix. Thus, the clay may have two competing roles regarding the thermal stability of nanocomposites: (i) a barrier effect, which should improve the thermal stability and (ii) a catalytic effect on the degradation of the polymer matrix, which should decrease the thermal stability. We suggest that the neat MMT catalyzed the degradation of the PH matrix.

Table III also reports the glass transition temperature T_g for the materials as determined by MDSC and confirmed by dynamic mechanical analysis (DMA). The neat polymer showed a T_g of 32°C. Strikingly, the protonated polymer exhibited a T_g of 155°C, an increase of over 120°C relative to the neat polymer. However, incorporation of the nanoclay up to 3 wt % further increased the T_g, some 10 to 15°C. The influence of nanoclay concentration on T_g is shown in Figure 4. Moreover, comparison of the T_g values of the nanocomposites with 3 wt % of clay with and without surfactants suggests that the use of ammonia induces an additional increase of T_g of $\approx$ 6°C (see Table III).

At relatively low concentrations of organo-MMT the nanometric secondary particles are easily exfoliated and uniformly dispersed in the polymer matrix, so that the exfoliation effect is relatively strong. In this case, the chemical interaction and the nanometer effect play key roles in obstructing the motion of polymer segments resulting in a significant increase in T_g.[2] It is assumed that ion-dipole interactions might be the driving force for the immobilization of the organic polymer chains lying flat on the layered silicate. Therefore, a cationic surfactant can induce interaction with the nanoplates thus stiffening the molecular chains, slowing the molecular dynamics and therefore increasing T_g.

However, we note that the sulfobetaine group in the surfactant C_{12}SB is an internal salt (i.e., its internal charges are neutralized), thus its interactions must be weaker than a cationic surfactant. Therefore, we suggest that C_{12}SB tends to act as a plasticizer for the polymer matrix and thus it induced a decrease in T_g. This observation is in agreement with results reported by Ke and Yongping,[17] who conducted thermal analysis on intercalated PET/*o*-MMT nanocomposites. Those authors reported a reduction of T_g in the composite compared to the neat polymer matrix, which they attributed to the plasticizing effect of *o*-MMT. Moreover, Fan et al. showed that the glass transition involves the freezing of large-scale molecular motion without a change in structure. Indeed, they showed that T_g is always lowered when adding modified MMTs.[18]

Figure 5 shows MDSC heating scans exhibiting the influence of nanoclay concentration on T_g when using sulfobetaine as surfactant. The results show a slight reduction of T_g with concentration. Furthermore, at 5 wt % the transition became broader.

The glass transition temperatures were further verified by means of DMA. Figure 6 shows a plot of mechanical damping Tan δ ($=G''/G'$) (where G' is the storage shear modulus and G'' the viscous shear modulus) as a function of temperature for (a) PDMAEMA, (b) PDMAEMAH, (c) PH/MMT/C_{12}SB 3 wt %, (d) PH/MMT/C_{12}SB 5 wt %, (e) PH/MMT 3 wt %, and (f) PH/MMT/$C_{14}NH_4^+$ 3 wt %. In dynamic mechanical temperature scans the glass transition temperature is not uniquely defined but is dependent of the frequency applied and it is also conventionally determined by either the onset in the

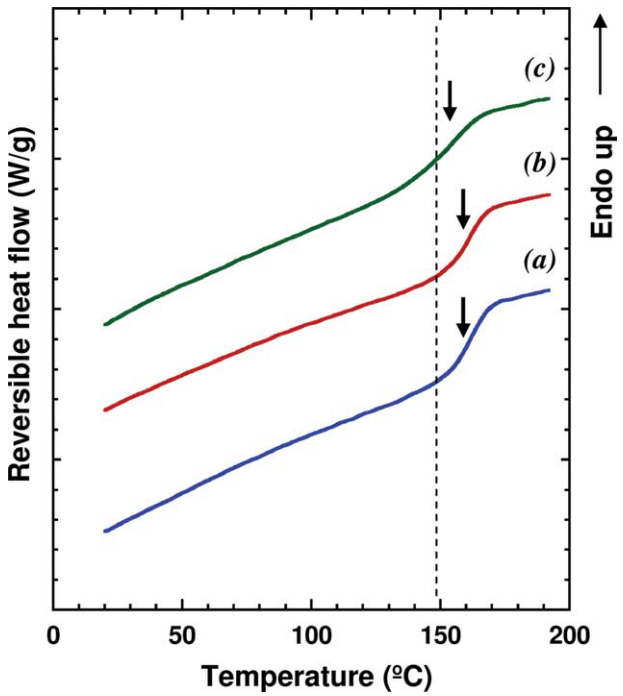

Figure 5 Modulated DSC heating scans of PDMAEMH layered silicate nanocomposites using sulfobetaine surfactant (PH/MMT/C_{12}SB). Nanoclay concentration of (a) 1, (b) 3, and (c) 5 wt %. Reversible heat flow obtained from second heating scan. [Color figure can be viewed in the online issue, which is available at wileyonlinelibrary.com.]

storage modulus G' ($T_{g,\,G'}$), the temperature at maximum in the loss modulus G'' ($T_{g,\,G''}$), or the temperature at maximum in Tan δ ($T_{g,\,\mathrm{Tan}\delta}$). The T_g values follow the order $T_{g,\mathrm{DSC}} = T_{g,\,G'} < T_{g,\,G''} < T_{g,\,\mathrm{Tan}\delta}$.[19] Table III lists the T_g values determined by DMA using the criteria of G''. The results of Figure 6 shows that the temperature at Tan δ_{max} for the polymer precursor PDMAEMA is ~ 50°C whereas for the protonated polymer PDMAEMAH is ~ 170°C, an increase of about 120°C, in agreement with the MDSC results (see Fig. 4). It is also noteworthy that the nanocomposite with the ammonia-treated clay exhibits the highest temperature at Tan δ_{max} of all the series, in accordance with the above reported MDSC measurements. This behavior should be a consequence of the intercalated morphology found for PH/MMT/$C_{14}NH_4^+$ 3 wt % in contrast to the exfoliated one in case of PH/MMT/C_{12}SB 3 wt %, as will be discussed below. The results also show that the maximum values of Tan δ for the protonated polymer, the SB-treated MMT and the neat MMT nanocomposites are smaller than for the precursor polymer indicating that there is less dissipation of energy in those materials. However, the ammonia-treated MMT showed the highest Tan δ values indicating the largest dissipation of energy among all the nanocomposites.

The increase in T_g upon addition of nanoclay suggests that there is some reduction in the mobility of the polymer chains. The origin of this hindered mobility could be twofold: first, it is suggested that the silicate layers interact with the polymer matrix through the ionic group. The interactions of the intercalated polymer chains with the host species would greatly reduce their rotational and translational mobility. The situation is similar to that in a reticulated polymer, where restrictions on its mobility increase the glass transition temperature (T_g).[1] A similar increase is anticipated to occur in a nanocomposite due to the increase of the energy threshold needed for the transition. It should be borne in mind that the increase in T_g is an important property of these materials that enables them to be employed at higher temperatures compared with the original polymer and thus extends their field of application.[1] Second, the molecular segment motion of the polymer out of the galleries of clay may be somewhat confined by the intercalated and exfoliated silicate layers, as suggested by Guo et al.[20] Figure 6 also shows that the samples with higher concentration of organo-MMT exhibited a slight reduction in T_g. This may be due to increased aggregation of organo-MMT in the composites as will be shown by the X-ray scattering results reported in next section.

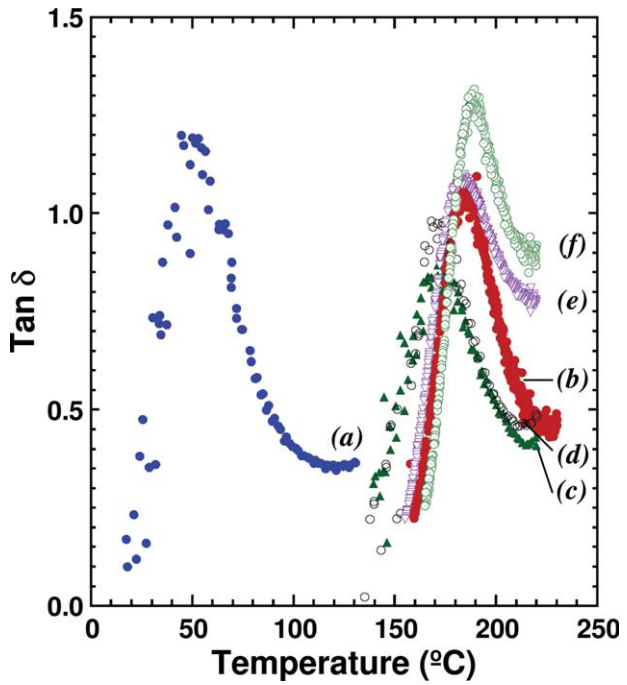

Figure 6 Mechanical damping Tan δ (= G''/G') as a function of temperature for (a) PDMAEMA, (b) PDMAEMAH, (c) PH/MMT/C_{12}SB 3 wt %, (d) PH/MMT/C_{12}SB 5 wt %, (e) PH/MMT 3 wt %, and (f) PH/MMT/$C_{14}NH_4^+$ 3 wt %. [Color figure can be viewed in the online issue, which is available at wileyonlinelibrary.com.]

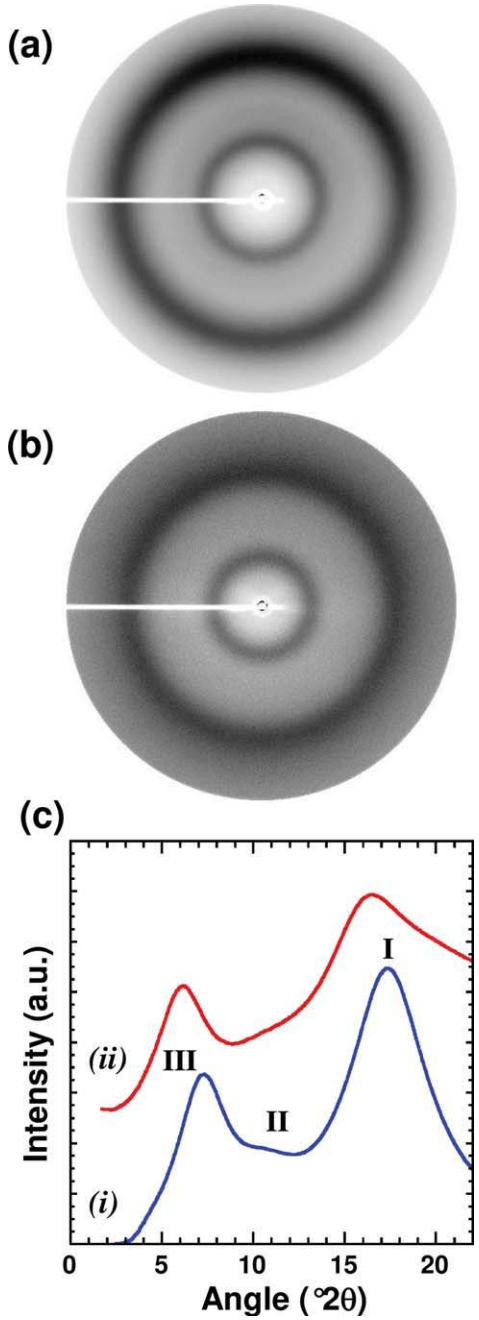

Figure 7 MAXS patterns of (a) PDMAEMA and (b) protonated PDMAEMA (PDMAEMAH). (c) Azimuthally averaged intensity traces of (i) PDMAEMA and (ii) PDMAEMAH. CuKα radiation. [Color figure can be viewed in the online issue, which is available at wileyonlinelibrary.com.]

Nanostructure via MAXS

Figure 7 shows the MAXS patterns of the (a) neat and (b) protonated polymer; whereas the corresponding azimuthally averaged intensity scans are shown in Figure 7(c). Isotropic rings are observed in Figures 7(a,b) suggesting that there is no preferential molecular orientation. Moreover, isotropic scattering was always found for the series of nanocomposites investigated.

PDMAEMA exhibits two well-defined amorphous halos located at $2\theta = 7.3^\circ$ and 17.4°. In addition, a weak maximum can be seen at $2\theta = 10.9^\circ$. The peaks are assigned in Figure 7(c) in accord with the literature found for other poly(*n*-alkylmethacrylates).[21–24] The diffraction curve of PDMAEMA resembles those observed for other amorphous (atactic) poly(methacrylates), especially in the case of long side chain groups such as *a*-poly(*n*-butylmethacrylate) (*a*-PBMA) and poly(*n*-hexylmethacrylate) (*a*-PHMA).[21] In the poly(methacrylate) series, peak I is usually associated to the mean van der Walls distance of not chemically bound atoms, with a corresponding "Bragg" spacing of $d_I = 0.5$ nm. In case of PDMAEMA, we find $d_I = 0.51$ nm. However, the presence of peak III at small scattering angles has been related to intersegmental connectivity of the side-chains. The structural model proposed for poly(*n*-alkylmethacrylates) consists in local layers of main chain segments parallel to each other and separated by layers of side chains.[21] In this scenario, peak III would arise as a consequence of the coherence length between side-chain domains. We find $d_{III} = 1.21$ nm for PDMAEMA, in good agreement with the values reported for *a*-PBMA and *a*-PHMA ($d_{III} = 1.2$–1.4 nm).[21–24] Finally, the weak maxima observed in the diffraction pattern of PDMAEMA at $2\theta = 10.9^\circ$ ($d = 0.81$ nm) [see Fig. 7(c)] coincides in position and intensity with peak II of long side-chain poly(alkylmethacrylates) ($d_{II} = 0.80$ nm). This peak has been associated to an intrasegmental distance between side chains.

The diffraction curve of the protonated polymer [trace ii in Fig. 7(c)] mainly differs from that of the pristine material in a shift of peak III towards smaller scattering angles. The "Bragg" spacings for peaks I and III (peak II is here difficult to resolve) are now: $d_I = 0.54$ nm and $d_{III} = 1.43$ nm. Hence, a significant increase of the d_{III} spacing is observed upon protonation. Previous published work in poly(*n*-alkylmethacrylates) show that d_{III} increases with increasing side-chain length, due to the fact that the coherent length between side-chain layers increases. In this case, the increase of d_{III} for the protonated material could be associated to the larger size of the side-group.

Figure 8 shows MAXS patterns of PH/MMT/$C_{14}NH_4^+$ nanocomposites containing (a) 1 and (b) 3 wt % nanoclay. As stated above, the patterns exhibit concentric rings indicating the absence of preferred molecular orientation in the nanocomposites. It can be seen that the nanocomposite containing 1 wt % nanoclay [Fig. 8(a)] shows only amorphous halos, which correspond to the polymer matrix. The loss of periodic spatial registry of the clay nanolayers

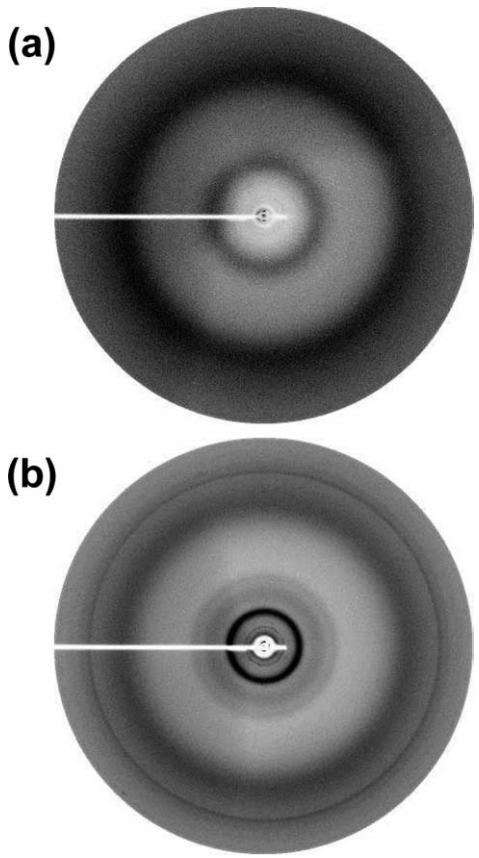

Figure 8 MAXS patterns of PH/MMT/$C_{14}NH_4^+$ nanocomposites containing (a) 1 and (b) 3 wt % nanoclay. CuKα radiation.

suggests that the nanoclay is exfoliated in the polymer matrix. However, the nanocomposite containing 3 wt % nanoclay [Fig. 8(b)] shows crystalline reflections in addition to the polymer matrix amorphous halos. The internal crystalline reflections are associated to the spatial registry of the nanoplates whereas the outer crystalline reflection corresponds to the internal crystalline structure of MMT.

The azimuthally integrated intensity traces of the nanocomposites containing 1 wt % and 3 wt % of MMT are shown in Figures 9(a,b), respectively. The diffraction curves of the protonated matrix (PDMAEMAH) and the neat MMT material are also included in Figure 9(a) for the sake of comparison. The Bragg spacings associated to the main peaks are included in Figure 9 for the sake of clarity. A strong peak at $2\theta = 7.1^\circ$ characterizes the gallery spacing of MMT (1.24 nm), while the maximum at $2\theta = 14.2^\circ$ corresponds to the gallery spacing second order reflection (0.62 nm). The peak at $2\theta = 19.7^\circ$ (0.45 nm) is associated to the internal crystal structure of the clay. The diffraction curves of the nanocomposites with 1 wt % of nanoclay are very similar for the two surfactants employed: two broad amorphous halos characterize the polymer matrix while a small peak at low scattering angles can be associated to the MMT gallery spacing (2.2 nm). The larger interlayer spacing with respect to neat MMT suggests the incorporation of polymer chains between clay plates. However, the weak intensity of these low-angle maxima (in case of ammonia surfactant the peak is only discernible as a shoulder) suggests that the majority of the nanoclay is dispersed in the polymer matrix and only a limited amount is forming part of an intercalated

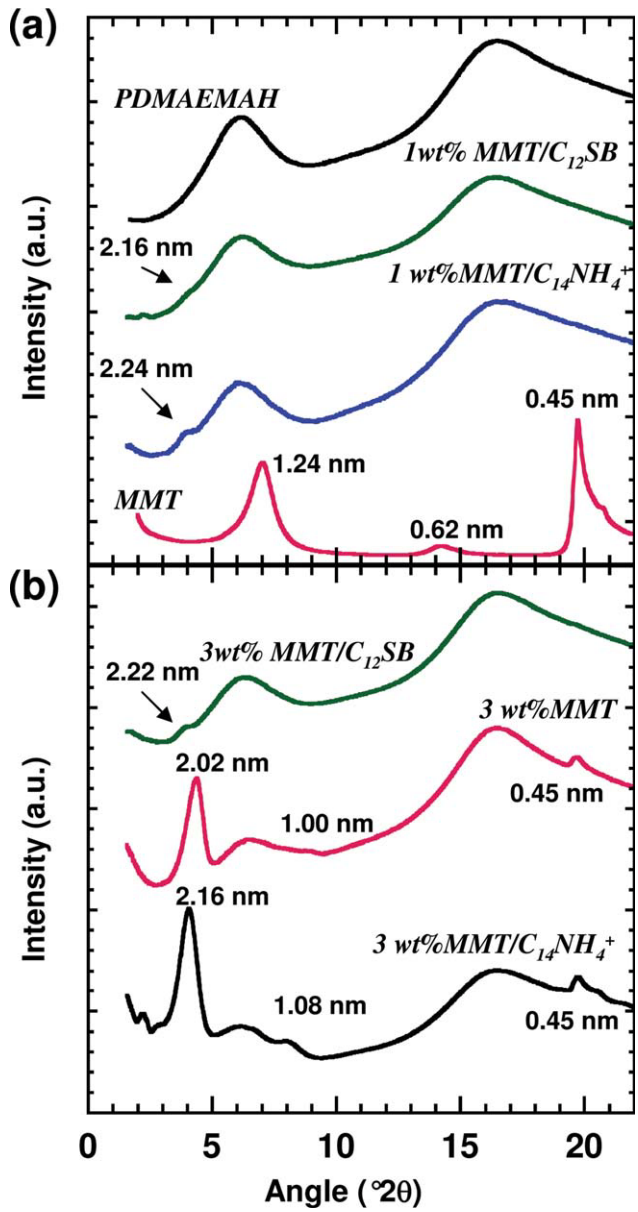

Figure 9 Azimuthally integrated MAXS intensity traces of the PDMAEMAH/MMT nanocomposites containing: (a) 1 wt % of MMT treated with ammonia or sulfobetaine surfactant). Intensity traces for the polymer matrix (PDMAEMAH) and the nanoclay (MMT) are also included for comparison. (b) 3 wt % of MMT, ammonia-treated MMT or sulfobetaine-treated MMT. Curves are shifted for the sake of clarity. [Color figure can be viewed in the online issue, which is available at wileyonlinelibrary.com.]

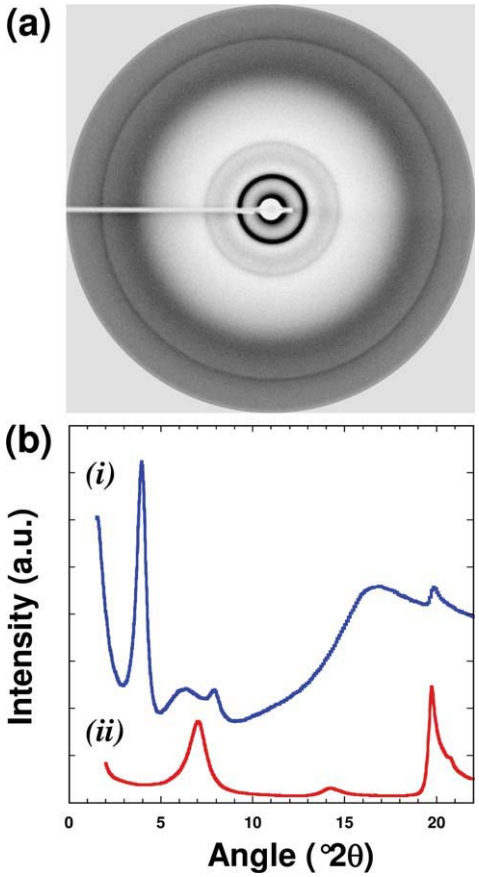

Figure 10 (a) MAXS pattern of PH/MMT nanocomposite containing 5 wt % nanoclay. (b) Azimuthally integrated MAXS intensity traces of PH/MMT (trace i) and that corresponding to MMT (trace ii). Curves are shifted for the sake of clarity. CuKα radiation. [Color figure can be viewed in the online issue, which is available at wileyonlinelibrary.com.]

morphology. Such structure is preserved for larger amounts of MMT up to 3% only in case that the sulfobetaine-based surfactant is employed [see Fig. 9(b)]. In contrast, the nanocomposite with 3 wt % of MMT treated with ammonia exhibits a marked intercalated character. Indeed, the peak associated with the gallery spacing of the nanoclay is here clearly defined in the diffraction curve and even exhibits a second order maximum. A similar diffraction curve is found for the nanocomposite prepared without surfactant [see Fig. 9(b)]. It should be noted that the clay gallery spacing is larger for the ammonia-treated clay than for the nanocomposite without surfactant. In addition, for both materials, the relative intensity of the amorphous halo located at $2\theta = 6.2^\circ$ with respect to the one at higher diffraction angle diminishes. As mentioned before, the amorphous halo at low diffraction angle has been associated to the coherence length between side-chain domains. Intercalation of the polymer material between the nanoclay plates would necessarily perturb the periodicity of these domains, of the order of 1 nm. Therefore, the intensity of the associated amorphous halo would decrease.

As suggested by the results presented above, increasing the concentration of nanoclay (neat and surfactant treated) further enhances polymer intercalation. Figure 10 shows the MAXS diffraction pattern (and corresponding azimuthally averaged intensity trace) of a nanocomposite containing 5 wt % MMT. The 001 reflection ($2\theta = 3.98^\circ$) corresponding to the gallery periodicity is greatly enhanced and even its second order 002 is clearly appreciated at $2\theta = 7.91^\circ$. The *d*-spacing correspond to 2.22 nm and 1.17 nm, respectively.

In summary, the sulfobetaine surfactant is found to promote exfoliation of the clay layered structure, in agreement with recent transmission electron microscopy observations.[14] This is also the case when low concentrations of ammonia treated clays are incorporated in the polymer matrix. However, for larger clay concentrations (>3 wt %), an intercalated nanostructure is predominant, regardless of the type of surfactant used. It is noteworthy that intercalated morphologies exhibited higher T_g values than exfoliated ones (see on Table III the T_g values of PH/3MMT and PH/MMT/3NH, intercalated structures, with respect to PH/MMT/3SB, exfoliated morphology), in agreement with our previous contention that intercalated polymer chains would exhibit hindered mobility.

Viscoelastic properties

The rheological behavior of the materials was investigated in the LVE regime. Applying strain sweeps at controlled frequency of 1 rad/s, we determined that the nanocomposites are linearly viscoelastic up to strains of $\sim 10\%$.

The dynamic moduli within the LVE regime were characterized by frequency sweeps carried out in a range of temperatures from 70 to 190°C for the neat polymer, and between 150 and 230°C for the protonated polymer and the nanocomposites. Logarithmic plots of $G'(\omega)$ and $G''(\omega)$ taken at temperature T were superimposed on those for temperature T_{ref} by a translation of the empirical shift factors log a_T along the frequency axis. No shifts along the modulus axis were required. Time-temperature reduction such as this can be expressed by[25]

$$G^{\#}(\omega, T) = G^{\#}(\omega \cdot a_T, T_{\text{ref}}) \quad (1)$$

where the symbol (#) stands for either one prime (′) or two primes (″). In this study, we chose a reference temperature, T_{ref} of 170°C.

The results showed that the neat polymer and the nanocomposites obeyed the time-temperature

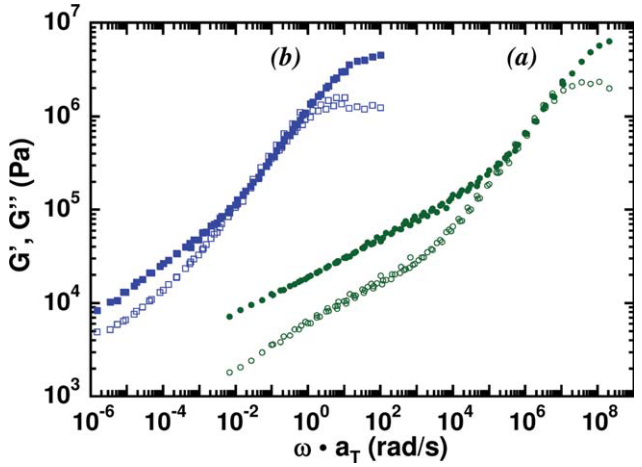

Figure 11 Shear moduli master curves as a function of strain rate of (a) PDMAEMA and (b) PH/MMT/C_{12}SB 3 wt %. Storage G′ (filled symbols) and viscous G″ (open symbols) dynamic shear moduli. T_{ref} = 170°C. [Color figure can be viewed in the online issue, which is available at wileyonlinelibrary.com.]

superposition principle (TTS). To emphasize the spectacular change in the thermal properties between the precursor polymer and the nanocomposites, Figure 11 shows, as an example, the master curves covering 15 decades in frequency of (a) PDMAEMA and (b) the nanocomposite containing 3 wt % sulfobetaine, PH/MMT/C_{12}SB. The results show that the precursor PDMAEMA exhibits the rubber-like regime ($G' > G''$), extending over seven decades in frequency. Increasing the frequency there is the transition regime (G'–G'') followed by the glass-like regime ($G' > G''$). The relatively low glass transition temperature of this material indicates that at room temperature it behaves as a soft sticky rubber. It can be seen that the nanocomposite PH/MMT/C_{12}SB also exhibits the rubber-like, transition and glass-like regimes. However, the main difference is that the master curve is shifted by about seven decades to much shorter frequencies (i.e., much longer relaxation times). This result is consistent with the significantly higher glass transition temperature exhibited by the nanocomposites.

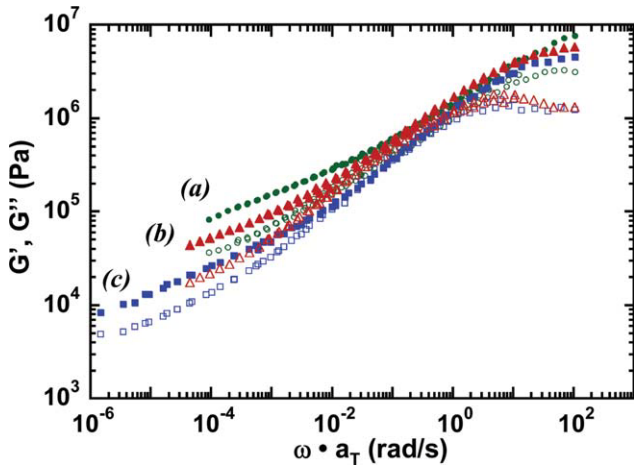

Figure 12 Shear moduli master curves as a function of strain rate of nanocomposites containing 3 wt % nanoclay. (a) MMT, (b) PH/MMT/$C_{14}NH_4^+$, and (c) PH/MMT/C_{12}SB. Storage G' (filled symbols) and viscous G″ (open symbols) dynamic shear moduli. T_{ref} = 170°C. [Color figure can be viewed in the online issue, which is available at wileyonlinelibrary.com.]

Figure 12 shows dynamic shear moduli master curves as a function of strain rate for the nanocomposites containing 3 wt % nanoclay: (a) MMT, (b) PH/MMT/$C_{14}NH_4^+$, and (c) PH/MMT/C_{12}SB. The results show that the dynamic moduli in the rubber-like regime are the highest for the untreated MMT [Fig. 12(a)] and the lowest for the SB-treated MMT [Fig. 12(c)]. These results are consistent with the nanostructure exhibited by these nanocomposites [see Fig. 9(b)]. The nanocomposite prepared with untreated MMT shows an intercalated morphology with the smallest layer spacing of the three nanocomposites. However, the SB-treated MMT exhibits the largest gallery spacing, and mostly exfoliated morphology. In other words, the molecular chains in the PH/MMT nanocomposite are more confined than the other two nanocomposites thus slowing down the macromolecular dynamics and giving rise to the higher rubber-like modulus.

CONCLUSIONS

Protonated N,*N*-dimethylaminoethylmethacrylate (PDMAEMAH)/organo-MMT nanocomposites have been prepared by solution casting technique. The protonated polymer exhibited an increase in glass transition temperature T_g of over 120°C relative to the neat polymer probably due to ionic interactions. Addition of nanoclay further increased T_g. The concentration as well as the type of surfactant used to treat the MMT influenced the nanostructure. Lower concentration and sulfobetaine surfactant favored exfoliation whereas ammonia and untreated MMT favored intercalation of the nanoplates. The modification of the polymer chain dynamics afforded by the state of confinement between the nanoplates slowed down the macromolecular dynamics as evidenced by changes in the rheological rubber-like modulus.

The authors thank Dr. Vicente Gariba y Flebes, Jorge Rocha, and Laboratorio de Docencia en Química, DCBI, UAM-I for their technical help. We are also indebted to the Department of Crystallography (Instituto Química-Física "Rocasolano," CSIC) for providing the facilities to carry out the X-ray diffraction experiments.

References

1. Pavlidou, S.; Papaspyrides C. D. Prog Polym Sci 2008, 33, 1119.
2. Sinha Ray, S.; Okamoto, M. Prog Polym Sci 2003, 28, 1539.
3. Fischer, H. Mater Sci Eng C 2003, 23, 763.
4. LeBaron, P. C.; Wang, Z.; Pinnavaia, T. J. Appl Clay Sci 1999, 15, 11.
5. Tjong, S. C.; Meng, Y. Z.; Hay, A. S. Chem Mater 2002, 14, 44.
6. Patel, H. A.; Somani, R. S.; Bajaj, H. C.; Jasra, R. V. Bull Mater Sci 2006, 29, 133.
7. Gilman, J. W.; Jackson, C. L.; Morgan, A. B.; Harris, R., Jr.; Manias, E.; Giannelis, E. P.; Wuthenow, M.; Hilton, D.; Phillips, S. H. Chem Mater 2000, 12, 1866.
8. Lan, T.; Pinnavaia, T. J Chem Mater 1994, 6, 2216.
9. Kroschurtz, J. S., Ed. For definitions and background on layered silicate and clay minerals, see: Kirk-Othmer Encyclopedia of Chem Technology, 4th ed.; John Wiley and Sons: New York, 1993; Vol. 6.
10. Bruce, P. G. Solid State Electrochemistry; Cambridge University Press: Cambridge, 1995.
11. Fan, L.; Nan, C. W.; Li, M. Chem Phys Lett 2003, 369, 698.
12. Appetecchi, G. B.; Croce, F.; Persi, L.; Ronci, F.; Scrosati, B. Electrochim Acta 2000, 45, 1481.
13. Croce, F.; Appetecchi, G. B.; Persi, L.; Scrosati, B. Nature 1998, 394, 456.
14. Cardoso, J.; Montiel, R.; Manero, O. J Appl Polym Sci 2011, 119, 1357.
15. Liu, X.; Wu, Q. Macromol Mater Eng 2002, 287, 180.
16. Zhao, C.; Qin, H.; Gong, F.; Feng, M.; Zhang, S.; Yang, M. Polym Degrad Stab 2005, 87, 183.
17. Ke, Z.; Yongping, B. Mater Lett 2005, 59, 3348.
18. Fan, L.; Ce-Wen, N.; Ming, L. Chem Phys Lett 2003, 369, 698.
19. Aklonis, J. J.; MacKnight, W. J. Introduction to Polymer Viscoelasticity, 2nd ed.; Wiley: New York, 1983, p 60.
20. Guo, B.; Ouyang, X.; Cai, C.; Jia, D. J Polym Sci Part B: Polym Phys 2004, 42, 1192.
21. Wind, M.; Graf, R.; Renker, S.; Spiess, H. W.; Steffen, W. J Chem Phys 2005, 122(1), 014906.
22. Miller, R. L.; Boyer, R. F.; Heijboer, J. J Polym Sci Polym Phys Ed 1984, 22, 2021.
23. Floudas, G.; Stepanek, P. Macromolecules 1998, 31, 6951.
24. Beiner, M.; Schröter, K.; Hempel, E.; Reissig, S.; Donth, E. Macromolecules 1999, 32, 6278.
25. Ferry, J. D. Viscoelastic Properties of Polymers; John Wiley and Sons: New York, 1980.